PROCEEDINGS, 41st Workshop on Geothermal Reservoir Engineering
Stanford University, Stanford, California, February 22-24, 2016
SGP-TR-177

Thermo-Poroelastic Effects on Reservoir Seismicity

Ahmad Ghassemi[1] , Qingfeng Tao[2]

[1]The University of Oklahoma, Norman, OK

[2]Weatherford International, Houston, TX

ahmad.ghassemi@ou.edu

Keywords: Enhanced geothermal system, displacement discontinuity, delayed seismicity, thermo-poroelasticity, shear slip

ABSTRACT

In this paper we consider the role of thermo-poromechanical processes on reservoir seismicity using theoretical/numerical analysis. The numerical model is fully coupled, considering non-isothermal compressible single-phase fluid flow in fractured porous rock. It combines the thermo-poroelastic displacement discontinuity method, a nonlinear joint deformation model, and a finite difference method for solving the fluid and heat transport in a fracture network. The model is applied to simulate cool water injection into fracture/matrix systems to examine the role of coupled processes on fracture deformation, matrix pore pressure and stress redistributions to assess their role in induced seismicity and permeability variations. The simulation results are analyzed to draw conclusions regarding injection rate dependence of seismicity, and its transience due to coupled processes. Thermal influence on pore pressure and stress tend to promote delayed seismicity. In the presence of coupled processes, rock matrix stress perturbations due to natural fracture deformation can be an influencing mechanism for seismicity. Our results show the induced normal stress in the vicinity of the fracture center where injected water enters, can be significant for higher cooling levels in low permeability matrix, and induces additional pore pressure perturbations in the matrix. These couplings have implications for reservoir stimulation and induced seismicity in geothermal reservoirs. The reservoir matrix can experience a series of induced stress regimes with continued cooling (under injection). An initially destabilizing regime is followed by a stabilizing one, and subsequently the rock approaches a destabilizing state. Each situation can result in potentially different levels of MEQ activity.

1. INTRODUCTION

Design and management of enhanced geothermal system (EGS) can benefit from simulation of coupled fracture deformation and fluid flow, because interactions among fluid and heat flow, and the mechanical response of the fracture and matrix impact reservoir performance and the occurrence of seismicity. The coupling between these processes can be taken into account using linear theory of thermo-poroelasticity. When the rock matrix permeability is low (Delaney, 1982) and fluid flows mainly within deformable fractures or a fault, conductive transport in the rock matrix leads to important phenomena related to coupling between temperature, pore pressure, and stress that may result in delayed rock matrix and/or natural fracture failure, potentially producing delayed seismicity.

Although the thermo-poroelastic constitutive equations are linear, analytical solutions can be found only for relatively simple geometries and processes (e.g., Tao and Ghassemi, 2010; Ghassemi et al. 2008) and the solution of problems such as injection/ extraction into a deformable fracture network requires numerical modeling even in two dimensions. In this work, a two dimensional displacement discontinuity model is used to examine important coupling mechanisms and their role on fracture deformation, and the stress state variations within the rock matrix. The model addresses the impact of fracture deformation and transport processes on the re-distribution of stress and pore pressure fields in the geothermal reservoir. The latter provides valuable insight on the role of coupled processes on induced seismicity.

2. PORO-THERMOELASTIC DISPLACEMENT DISCONTINUITY METHOD (DDM)

The constitutive equations of the linear theory of thermos-poroelasticity are: (McTigue, 1986):

$$\varepsilon_{ij} = \frac{1}{2G}\left[\sigma_{ij} - \frac{v}{1+v}\sigma_{kk}\delta_{ij}\right] + \frac{\alpha(1-2v)}{2G(1+v)}\delta_{ij}p + \frac{\alpha_s}{3}\delta_{ij}T \qquad (1)$$

$$\zeta = \frac{\alpha(1-2v)}{2G(1+v)}\sigma_{kk} + \frac{\alpha^2(1-2v)^2(1+v_u)}{2G(1+v)(v_u-v)}p - \phi(\alpha_f - \alpha_s)T \qquad (2)$$

where ε_{ij} and σ_{ij} are the change of strain and stress of the solid matrix, respectively, p and ζ are the change of pore pressure and pore volume respectively, T is the change of temperature and δ_{ij} is the Kronecker delta. The material constants are the bulk shear modulus G, Biot's coefficient, α, the drained and undrained Poisson's ratios v and v_u, Skempton's pore pressure coefficient B, and the volumetric

thermal expansion coefficients of the solid matrix α_s and the pore fluid α_f. This version of the theory is suitable for when convective heat transport can be neglected in the porous matrix. Despite this simplifying assumption, the equations of the theory are generally not amenable to analytical solutions and require numerical modeling, particularly when considering fractures. The thermos-poroelastic extension of the elastic (Crouch and Starfield, 1981) and poroelastic (Curran and Carvalho, 1987) displacement discontinuity method (Ghassemi and Zhang, 2004) has proven suitable for this purpose. The method has been developed based on Betti's reciprocal theory for thermos-poroelasticity.

Considering a thin fracture segment of length of *2a* in a porous matrix of infinite extent, the pore pressure and stress induced by a normal deformation ΔD_n, shear deformation ΔD_s, fluid injection Δq_{int} (the leakoff rate per fracture length), and heat flow rate $\Delta q_{h\text{-}int}$ (the interface heat flow rate per fracture length) at a point (*x, y*) at time t are obtained by summing the fundamental solutions and (Ghassemi and Zhang, 2006):

$$\Delta p(x,y,t) = p^{dn}(x,y,t)\,\Delta D_n + p^{ds}(x,y,t)\,\Delta D_s + p^{q}(x,y,t)\,\Delta q_{\text{int}} + p^{T}(x,y,t)\,\Delta q_{h-\text{int}} \quad (1)$$

$$\Delta \sigma_{ij}(x,y,t) = \sigma_{ij}^{dn}(x,y,t)\,\Delta D_n + \sigma_{ij}^{ds}(x,y,t)\,\Delta D_s + \sigma_{ij}^{q}(x,y,t)\,\Delta q_{\text{int}} + \sigma_{ij}^{T}(x,y,t)\,\Delta q_{h-\text{int}} \quad (2)$$

where the superscripts *dn*, *ds*, *q* and *T* denote normal displacement discontinuity source, shear displacement discontinuity source, fluid and heat source, respectively. The induced temperature *T* at any point (*x, y*) and time is only dependent on the heat source $q_{h\text{-}int}$ and the effects of D_n, D_s, and q_{int} are neglected (Eq. 3)).

$$\Delta T(x,y,t) = T^{T}(x,y,t)\,\Delta q_{h-\text{int}} \quad (3)$$

For a multi-fracture system, there are interactions among fracture segments. The induced temperature, pore pressure, normal and shear stress on the *ith* fracture segment by all fracture segments can be obtained by using the spatial and temporal superposition of the fundamental solutions:

$$\Delta T^{i}(t) = \sum_{j=1}^{m} T^{ij}(t)\,\Delta q_{h-\text{int}}^{j} \quad (4)$$

$$\Delta p^{i}(t) = \sum_{j=1}^{m} p^{ij\,dn}(t)\,\Delta D_n^{j} + \sum_{j=1}^{m} p^{ij\,ds}(t)\,\Delta D_s^{j} + \sum_{j=1}^{m} p^{ij\,q}(t)\,\Delta q_{\text{int}}^{j} + \sum_{j=1}^{m} p^{ij\,T}(t)\,\Delta q_{h-\text{int}}^{j} \quad (5)$$

$$\Delta \sigma_n^{i}(t) = \sum_{j=1}^{m} \sigma_n^{ij\,dn}(t)\,\Delta D_n^{j} + \sum_{j=1}^{m} \sigma_n^{ij\,ds}(t)\,\Delta D_s^{j} + \sum_{j=1}^{m} \sigma_n^{ij\,q}(t)\,\Delta q_{\text{int}}^{j} + \sum_{j=1}^{m} \sigma_n^{ij\,T}(t)\,\Delta q_{h-\text{int}}^{j} \quad (6)$$

$$\Delta \sigma_s^{i}(t) = \sum_{j=1}^{m} \sigma_s^{ij\,dn}(t)\,\Delta D_n^{j} + \sum_{j=1}^{m} \sigma_s^{ij\,ds}(t)\,\Delta D_s^{j} + \sum_{j=1}^{m} \sigma_s^{ij\,q}(t)\,\Delta q_{\text{int}}^{j} + \sum_{j=1}^{m} \sigma_s^{ij\,T}(t)\,\Delta q_{h-\text{int}}^{j} \quad (7)$$

where *m* denotes the total number of fracture segments, the over script *ij* denotes the influence of *jth* fracture segment on the *ith* fracture segment, and the over script *j* denotes the source strength of *jth* fracture segment. To consider the time variation of the discontinuities strengths (ΔD_n, ΔD_s, Δq_{int} and $\Delta q_{h\text{-}int}$), we use a time marching scheme to discretize the source strengths into step increments (see Ghassemi and Tao, 2016).

3. FLUID TRANSPORT IN FRACTURES

The aperture of real fracture varies in space and the fluid flow inside can also very complicated due to the rough surfaces. But Darcy's law is still considered valid and the rough fracture can be represented by a fracture with the average fracture aperture (Witherspoon et al. 1980). The coupled fluid flow equation (Eq. (8)) for a fracture-matrix system can be written as (Tao et al. 2010):

$$\frac{k_f w_f}{\mu}\nabla^2 p = 2a w_f c_f \frac{\partial p}{\partial t} - 2a\frac{\partial D_n}{\partial t} + 2a q_{\text{int}} + q_s \quad (80)$$

where k_f is the fracture permeability (k_f=w_f^2/12), w_f is the fracture aperture, μ is the fluid viscosity, c_f is the fluid compressibility, and q_s is the source term (injection or production).

4. HEAT TRANSPORT IN FRACTURES

The energy conservation equation in a fracture-matrix system is built by considering the rate of internal energy, ΔU, the heat flow rate at the interface between fracture and matrix, $Q_{h\text{-}int}$, rate of energy change by conductive transport within the fracture, ΔE_d, and the energy

change rate by convective transport in fracture, ΔE_v. For a fracture segment of length of $2a$ with an aperture w_f, in a fracture-matrix system of unit thickness, the rate of internal energy change only results from the temperature change if the influence of the change of fracture aperture and fluid density are negligible. As a result, the energy conservation equation in a fracture-matrix system is given by (Tao and Ghassemi, 2010):

$$2a\, w_f \rho_w c_w \frac{\partial T}{\partial t} = k_T w_f \nabla^2 T - 2a\, \rho_w c_w q_f \nabla T - 2a q_{h-\mathrm{int}} \tag{11}$$

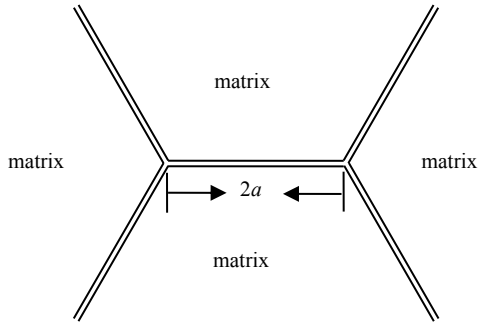

Figure 1: Illustration of a fracture segment in a fracture-matrix system.

5. FRACTURE DEFORMATION

The change of normal and shear stress acting on the fracture segment induces normal and shear deformation. To simulate this response of a rough fracture, the Barton-Bandis (1983) joint deformation model is applied in this study. In this model, the normal stress is a hyperbolic function of the normal closure:

$$\sigma_n' = \frac{K_{ni} D_n}{1 - D_n / D_{n\max}} \tag{12}$$

where σ_n' is the effective normal stress. But when the fracture deformation is small, the change of stress with the fracture closure can be approximated as a linear relation, $\Delta \sigma_n' = -K_n \Delta D_n$. The change of shear stress has a linear relationship with the change of shear displacement before yielding is $\Delta \sigma_s = K_s \Delta D_s$ where K_s is the shear stiffness. The fracture slips when the shear stress exceeds the shear strength (σ_c) of the fracture. We use an approximate linear relation for the aperture increase ($\Delta D_{n\text{-dilation}}$) in response to shear movement $\Delta D_{n-dilation} = -\Delta D_s \tan \phi_d$, where ϕ_d is the dilation angle.

6. SOLUTION METHOD

The fluid flow equation for a given fracture network is discretized in space and time using an implicit finite difference method. For the i^{th} fracture segment at the time step, ξ, the discretized fluid diffusivity equation is:

$$\sum_{j=1}^{m} C_p^{ij} p^j(t) - 2a\Delta D_n^{i\xi} + 2a\Delta q_{\mathrm{int}}^{i\xi} = 2a w_f c_f p^i(\tau_\xi) - 2a \sum_{h=0}^{\xi-1} \Delta q_{\mathrm{int}}^{ih} - \sum_{h=0}^{\xi} q_s^{ih} \tag{13}$$

where C_p^{ij} is the fluid coefficient matrix (Tao, 2010), which represents fluid diffusion in the fracture network. Similarly, the heat transport equation can be discretized in space and time for a given fracture network.

$$\sum_{j=1}^{m} C_{ht}^{ij} T^j(t) + 2a\Delta q_{h-\mathrm{int}}^{i\xi} = 2a\, w_f \rho_w c_w T^i(\tau_\xi) - 2a \sum_{h=0}^{\xi-1} \Delta q_{h-\mathrm{int}}^{ih} \tag{14}$$

where C_{ht}^{ij} is the coefficient matrix for heat transport in fractures representing heat transport in the fracture network. The C_{ht}^{ij} is dependent on the fluid flow rate, q_f, in the fractures.

7. MODEL APPLICATION

The objective is to illustrate the role of coupled thermo-poroelastic processes (related to water injection) on natural fracture opening and shear deformation, as well as on pore pressure and stress redistributions in the neighborhood of the natural fractures. Consider the 2D plane strain problem of a fracture oriented at 45 in the xy plane. The fracture is 40 m long under the action of in-situ stresses as shown in Figure 2. The initial pore pressure is 10 MPa and the rock/fracture system is at an initial temperature of 420 K. The rock matrix is assumed to be Westerly granite with other properties shown in Table 1.

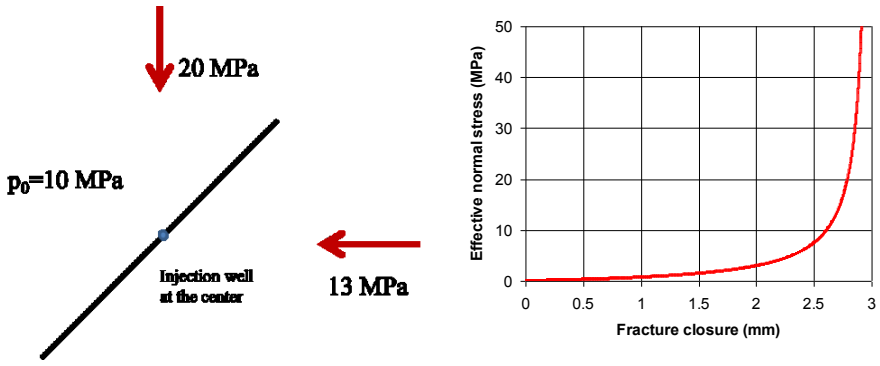

Figure 2: (a) Problem geometry and (b) the Barton-Bandis fracture model used. The fracture is 40 m long and the injection well is located at its center.

Shear modulus G (GPa)	15
Poisson's ratio υ	0.25
Undrained Poisson's ratio υ_u	0.33
Matrix permeability (m^2)	4×10^{-19}
Matrix porosity ϕ	0.01
Biot's coefficient α	0.44
Fluid viscosity μ (Pa.s)	2.037×10^{-4} at 400º 3.547×10^{-4} at 320º
Fluid compressibility (MPa^{-1})	4.2×10^{-4}
Thermal expansion coefficient of solid β_s (K^{-1})	2.4×10^{-5}
Thermal expansion coefficient of pore fluid β_f (K^{-1})	2.1×10^{-4}
Thermal diffusivity of intact porous rock c^T (m^2/s)	1.1×10^{-6}
Fluid density ρ_f (Kg/m^3)	1×10^3
Heat capacity of fluid c_w ($J\ kg^{-1}\ K^{-1}$)	4200

Table 1. Rock properties of Westerly granite (compiled from McTigue, 1986).

In this study, the natural fracture is modeled using the non-linear fracture closure model (Goodman, 1976, Bandis et al. 1983; Barton et al. 1985) fracture mechanical deformation model (Figure 9b) for opening and closure, and a linear shear deformation model. The fracture models are implemented in a thermo-poroelastic fracture network flow and deformation displacement discontinuity code as previously described. The fracture is in equilibrium with prescribed stress and pore pressure, and temperature conditions and has an aperture of 0.5623 mm. This is the actual fracture aperture under reservoir conditions and is calculated in the model internally using the prescribed initial fracture stiffness and stress state. The maximum fracture closure is 3 mm. Injection begins at time t=0+ at a constant rate specified in Table 2.

Initial reservoir temperature (K)	420
Injection water temperature (K)	400, and 340
Initial joint normal and shear stiffness, k_n , k_s (GPa/m)	0.5; 50
The maximum joint closure, D_{cmax} (mm)	3.0
Fracture aperture initial, D_{ni} (mm)	0.563
friction angle (ψ), (effective); cohesion (c), (MPa)	30; 0
In-situ stress (MPa) – y direction	20
In-situ stress (MPa) – x direction	13
Initial reservoir pore pressure (MPa)	10
Injection rate (m^3/s) /m thickness of reservoir	0.6×10^{-7}

Table 2. Data used in fracture simulations.

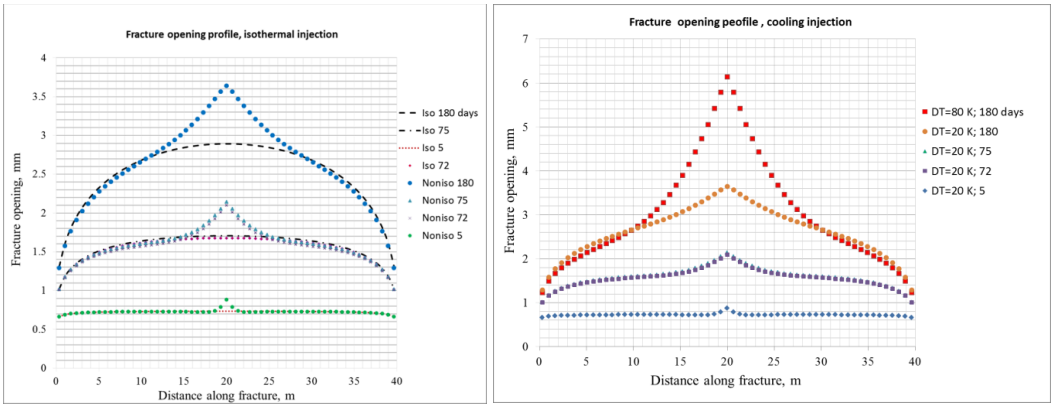

Figure 3: Fracture opening for different injection cases. Left: impact of time and comparison with isothermal case. Right: Impact of injection temperature and time.

All deformations resulting from thermal, pore pressure, and flow are mechanical deformations and result in fracture aperture variations. No distinction is made between hydraulic aperture and mechanical aperture in these simulations. If needed, one could specify a small residual aperture for flow purposes when the fracture is mechanically closed. Water viscosity in the following simulations is calculated for the average system temperature. The injection water temperature is specified as 400 K (a second case with injection water temperature 350 K is also presented). The problem is solved by dividing the fracture into 59 constant (in time and space) boundary elements. The solution time is divided into 60 (variable) steps. The fracture profiles in response to injection under different conditions are shown in Figure 3.

Figure 3 illustrates that cooling tends to increase the fracture aperture, however, in view of the low temperature contrast (ΔT) between the injection water and the rock, and the low value of thermal diffusivity, thermal stress is relatively small and develops very slowly. The thermal stress effect is localized in the central region of the fracture where most of the cooling occurs, and it expands with time. Increasing ΔT, increases the cooling-induced fracture opening**.** Note also the contrast between the profiles for the isothermal and cooling cases. Note that cooling in the fracture is controlled by the residence time of the fluid which is influenced by injection rate, leak-off, and fracture permeability.

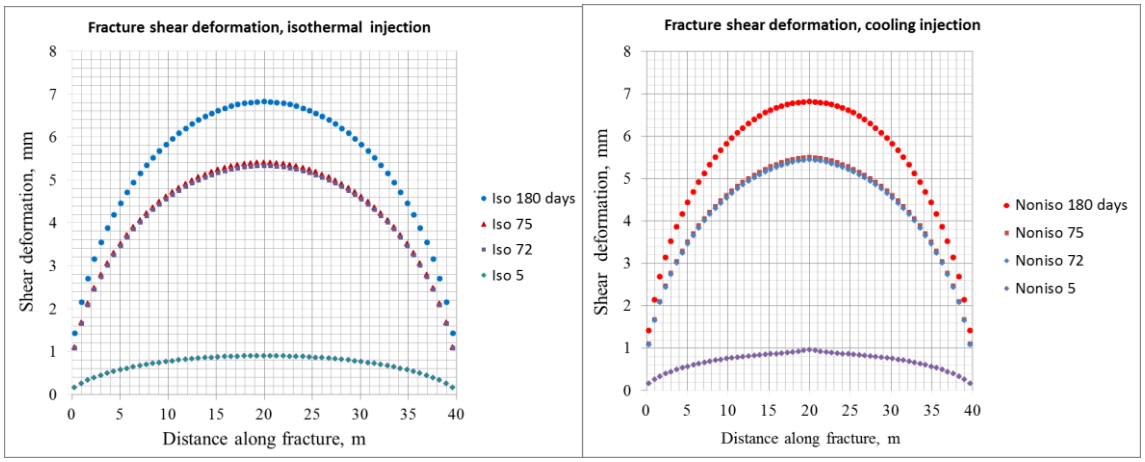

Figure 4: Shear deformation along the fracture. Results or isothermal (left) and cooling cases (right).

The distributions of shear deformation (elastic and permanent) are shown in Figure 4. The early evolution of the shear deformation is impacted by injection and cooling. It is interesting to note the reduction in the central element's normal stress and thus a lowering of its shear strength, causing an increase in the initial shear deformation at the fracture center. The associated shear slippage could generate micro-seismicity with increasing magnitude in time.

7.1 Evolution of pore pressure and stress in the vicinity of the fracture

Figure 5 shows the pore pressure evolution at a point in the rock matrix 0.5 m away from the fracture center. Pore pressure in the rock matrix tends to gradually increase in response to injection into the fracture, but the increase is not monotonic and episodes of pore pressure rise and drop are observed. This is because the pore pressure responds to three driving mechanisms: fracture opening

and poroelastic deformation of the rock matrix, pressure diffusion, and cooling of the fluid/matrix. For isothermal injection, the pore pressure changes are small at early times when the leak-off volume still is small. Note the trend for cooling by 20 K is similar to that of isothermal case except for large times when a small reduction in induced pore pressure is observed in comparison to the isothermal case. This is because leak-off is dominant. The matrix pore pressure for the case of cooling (20 K) injection into an impermeable fracture ("Cooling, Imp.") confirms this, showing a drop in pore pressure in response to cooling of the fluid/rock system.

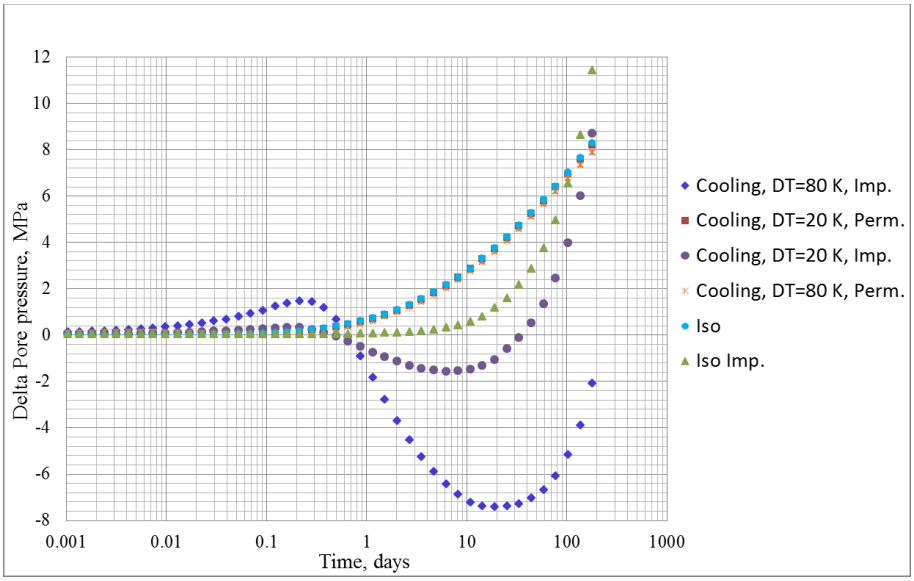

Figure 5: Induced pore pressure history in the rock matrix a point in the rock matrix 0.5 m away from the fracture center. Q=0.6x10^{-7} (m3/s) /m thickness of reservoir and viscosity= 2.037x10^{-04} Pa.s. The initial peak in pore pressurre can be explained by matrix compression associated with natural fracture opening in response to injection cooling. This peak is not observed for the isothermal injection case as the fracture opening is minimal in that case. Note from the "Cooling, DT=80, Imp" curve that cooling effect on pore pressure itself, tends to dominate the induced pore pressure from about 0.4 days to 250 days. The peak of pore pressure change propgates into the rock with time but its intensity is reduced with distance. The lower the matrix permeability, the stronger the coupling effects on pore pressure.

The isothermal injection case with a nearly impermeable matrix ($0.4x10^{-26}$ m^2) is worth noting. In this case, the pore pressure change is caused only by the volumetric rock deformation associated with fracture opening and the resulting matrix compression (the Skempton's pore pressure coefficient is 0.81). The case where rock matrix is impermeable and cooling injection is carried out is also very interesting. The pore pressure tends to increase in response to elastic compression of the fracture wall rock, but the thermal coupling causes the pore pressure to decrease (from 0.3-23 days), followed by an increasing trend as the cooling front passes through and pressure builds up in the fracture.

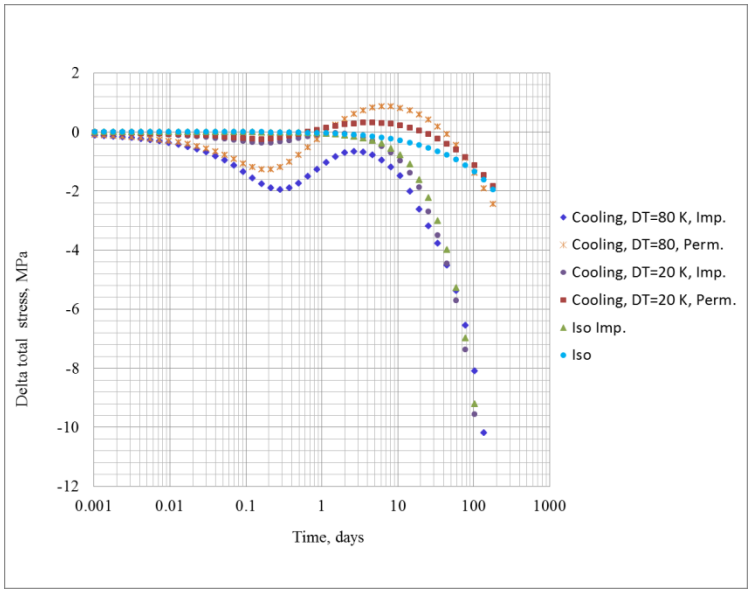

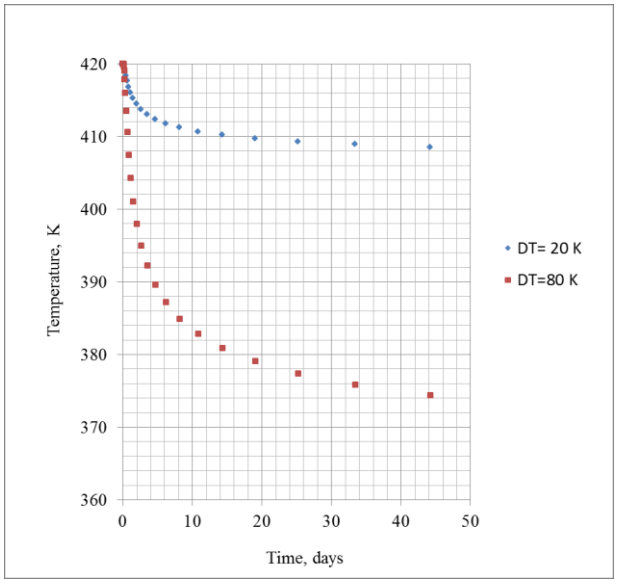

Figure 6: (a) History of induced normal stress, perpendicular to the fracture, (top) and temperature (bottom) at a point in the rock matrix 0.5 m away from the fracture center. The lower the matrix permeability, the stronger the stress shadow and its stress effects on pore pressure, and the stronger the thermal effect on stress.

The pore pressure reduction occurs ahead of the cooled zone and is a distinct consequence of thermo-poromechanical coupling inside the rock matrix (see e.g., Tao and Ghassemi, 2010). This phenomenon is more conspicuous for the case of 80 K injection cooling. Note that pore pressure tends to rise in the beginning in response to fracture (element) opening at the injection well. But then, cooling dominates and causes a substantial reduction in pore pressure before leak-off prevails and the pore pressure begins to increase (at about 24 days).

The distribution of induced total normal stress (stress component perpendicular to the fracture) at a point in the rock matrix 0.5 m meters away from the fracture center is shown in Figure 6. The pattern is similar to that of pore pressure variation and is highly impacted by matrix permeability and thermo-poroelastic effects. The total normal stress in the rock matrix increases in response to fracture opening and the poroelastic stress associated with pore pressure increases (0.001-0.3 days). Then, it decreases (0.3-3 days) with further cooling (induced tension) before increasing rapidly with further fracture opening in response to the applied pressure and poroelastic stress. Note that for the more permeable cases, the induced stress is tensile (from 1-50 days) whereas for less permeable cases, the induced stress is compressive (dominated by fracture wall compression).

8. DISCUSSION AND CONCLUSIONS

Reservoir stimulation is often accompanied by multiple micro-seismic events whose distribution and pattern are used to ascertain the extent of the stimulated volume and fracture growth, resulting reservoir permeability, and geometry of the geological structures and the in-situ stress state in EGS (Pine and Batchelor, 1984; Julian et al., 2006). The occurrence of seismicity in conventional geothermal fields, and the existence of a temporal relationship between injection/extraction operations and the occurrence of earthquakes have been known for many years (e.g., see Majer et al. 2007). Interpretation of micro-seismic events indicate rock failure in shear, and shear slippage on newly formed or pre-existing fracture planes (Pine and Batchelor 1984; Pearson, 1981) as well as tensile fracture initiation (Julian et al. 2010, Jung 2013). Both of these failure modes can be related to injection induced pore pressure increases in a critically-stressed rock and/or fractures. Evans et al. (2012) have documented and reviewed 41 European case histories of seismic response of crystalline and sedimentary rocks to fluid injection and no correlation was readily observed between the MEQ (micro-earthquake) magnitude and stress criticality. The indication is that in addition to critical stress levels, other rock mass conditions and processes contribute to MEQ. The fundamental mechanisms in reservoir seismicity are still not adequately understood and several key questions remain unresolved in the analysis of micro-seismicity, namely the variation of seismic activity with injection rate, delayed micro-seismicity, the relation of the stimulated zone to the injected volume and the injection rate, the connectivity of the fractures hosting micro-seismic events and the resulting reservoir permeability. The simulations presented herein, do shed some light on these unresolved questions and underscore the role of thermo-poromechanical processes: not only in changing fracture permeability, but also in induced seismicity.

The example injection simulations presented illustrate that injection pressure, fracture opening, as well as rock matrix deformation are sensitive to the injection rate. As injection rate increases, the pressure builds up in the fractures causing them to open more rapidly (and

ultimately to propagate). The higher pressure induces a higher stress and pore pressure in the reservoir matrix with potential for induced seismicity at early times. Compressing the surrounding rock and increasing its pore pressure can cause slippage on other favorably-oriented fractures (e.g, Safari and Ghassemi, 2015). On the other hand, a faster injection rate increases the cooling effect on the rock matrix stress and pore pressure compared to a slower injection case (see Ghassemi and Cheng, 2001). This is because more fluid is injected for a faster injection case in a given time period. A larger segment of the fractured is cooled off with a higher injection rate (a continuous high injection rate approaches the case of uniformly cooled fracture because the water temperature at one fracture face element does not change much when it reaches the next face element), lowering the matrix pore pressure over a larger region near the fracture walls and potentially decreasing the size of the slip zone and the MEQ activity. When injecting slower, a smaller region is cooled off so that a larger zone will remain at relatively higher pore pressures with a higher potential for failure. These effects are transient and with the passage of time, a continuously moderated low pore pressure peak propagates into the rock and pore pressure will eventually be controlled by leakoff. The above discussion pertains to the rock matrix response; clearly increased cooling (thermal stress) has a destabilizing effect on the main fracture or fractures that are subjected to direct water injection.

The potential contribution of coupled thermo-poroelasticity to seismicity (and delayed seismicity) are clearly illustrated in Figures 5-6. For the granitic rock type considered, fluid diffusivity is an order of magnitude higher than thermal diffusivity so that thermal stress effects tend to develop later than pore pressure effects. The pore pressure effects of cooling the rock, however, occur fast but could be short-lived depending on fluid diffusivity of the rock. Two important poroelastic effects are the pore pressure increase by volumetric deformation (rock compression through fracture pressurization) and pore pressure diffusion with the associated poroelastic stress. When the rock is cooled, the coupling between pore pressure and temperature also has a major role. In a system where there are fractures of highly variable apertures, it is expected that water would flow mostly in the more permeable pathways leading to further channeling of flow in the main fractures (heterogeneity in natural fracture aperture and stiffness can also cause channeling as shown in Rawal and Ghassemi, 2014).

The results show a very interesting phenomenon for the case of very low permeability rocks and/or cases of relatively high thermal perturbation. Early on in time, the pore pressure increase near the natural fracture (e.g., at a distance of 0.5 m) is about 2 MPa for the rock/fracture system considered. This is mainly a poroelastic effect wherein rock matrix compression associated with natural fracture opening (in response to local cooling), causes pore pressure to increase (see Figure 5). The magnitude of this pore pressure increase becomes larger with increasing injection rate, higher ΔT, and would also penetrate deeper into the rock matrix. The implication is that a higher injection rate tends to enhance MEQ potential in the vicinity of the injection fracture early on in time.

However at later times, a stabilizing effect is observed on the rock matrix and on critically-stressed natural fractures (in the vicinity of the main fracture) due to dominance of the thermo-poromechanical processes associated with cooling of the matrix: causing the pore pressure to substantially decrease (in the rock matrix) after experiencing the initial increase. With time, the reduction reaches as much 8 MPa after more than a month of injection (Figure 5). As time proceeds further, the pore pressure is restored to the initial level and then continually increases with leakoff into the matrix. The implication is that seismicity associated with pore pressure increase could be mitigated by cooling for some time. The pore pressure reduction is a distinct consequence of thermo-poromechanical coupling inside the rock matrix (see Ghassemi and Zhang, 2006 and Tao and Ghassemi, 2010) and its transience has not been noted in previous works such as Segall and Fitzgerald (1998) and Mossop (2001). As pointed out earlier, poromechanical and thermo-mechanical processes occur at different time scales, depending on the problem of interest and the rock mass properties. Therefore, the delayed response described above would depend on in-situ reservoir conditions and operations.

Our results (Figure 6) show that the induced total normal stress in the rock matrix (normal to the fracture, i.e., axial stress) away from the fracture center can be large. The total stress in the rock matrix increases in response to fracture opening, and the poroelastic stress associated with pore pressure increases (Figure 6), but further cooling and arrival of the cooling front decreases the stress by inducing a tensile stress. Later, the normal stress continues to increase rapidly in response to further fracture pressurization and opening, and pore pressure increase (see Figures 5 and 6) as the fracture transitions into a "hydraulic fracture." For relatively higher permeability rocks and higher cooling rates, a zone of tensile stress develops for some time which can produce tensile MEQ.

In summary, thermo-poromechanical coupling has major implications for reservoir stimulation and induced seismicity in geothermal reservoirs. These couplings cause the reservoir to experience a series of stress perturbations with injection. An initial destabilizing stage is followed by a stabilizing stage, after which another destabilizing stress regime is reached; each potentially impacting the MEQ activity. The thermo-poroelastic effects on reservoir seismicity can be viewed from two related standpoints: (a) the impact on the reservoir in-situ stress state and (b) the influence on the local fracture and fracture zone behavior with emphasis on fracture opening, slip, and/or propagation. Both have been illustrated herein. The former aspect is significantly influenced by coupled processes and should be included in assessment of induced seismicity. Consideration of only injected volume is not adequate for understanding the spatio-temporal distribution of injection related MEQ.

ACKNOWLEDGEMENTS

This work was partially supported by the U.S. Dept. of Energy Geothermal Technologies Office, the Code Comparison Study project.

REFERENCES

Barton N.R., Bandis S, Bakhtar, K. 1985. Strength, deformation and conductivity coupling of rock joints. International Journal of Rock Mechanics & Mining Sciences & Geomechanics Abstracts 22, 121–140.

Bandis, S.C., Lumsden, A.C. and Barton, N.R. 1983. Fundamentals of Rock Joint Deformation. International Journal of Rock Mechanics & Mining Sciences & Geomechanics Abstracts 20 (6), 249-268.

Bodvarsson G, Lowell R.P. 1972. Ocean-floor heat flow and the circulation of interstitial waters. Journal of Geophysical Research 77:4472–5.

Bruel, D. 2002. Impact of induced thermal stresses during circulation tests in an engineered fractured geothermal reservoir; example of the Soultzsus-Forets European Hot Fractured rock Geothermal Project, Rhine Graben, France. Oil and Gas Science & Technology Review, IFP, 57, 459–70.

Cheng, A. H.-D., and Ghassemi, A. 2001. Effect of fluid leak-off on heat extraction from a fracture in hot dry rock. Resources Council Conf., San Diego, CA.

Crouch S.L., and Starfield, A.M. 1983. Boundary element method in solid mechanics. George Allen & Unwin London.

Curran, J.H., and Carvalho, J.L. 1987. A displacement discontinuity model for fluid-saturated porous media. Proceedings of the 6th Congress of the ISRM, v.1, Montreal, pp. 73–78.

Delaney, P.T. 1982. Rapid intrusion of magma into wet rock: groundwater flow due to pore pressure increases. Journal of Geophysical Research 87(B9), 7739-7756.

DiPippo, R. 2012. Geothermal Power Plants: Principles, Applications, Case Studies and Environmental Impact, Elsevier Science, 3rd Edition. 624 pp.

Evans, K.F., Zappone, A., Kraft, T., Deichmann, N., Moia, F. 2012. A survey of the induced seismic responses to fluid injection in geothermal and CO2 reservoirs in Europe. Geothermics 41, 30-54.

Fredrich J.T., and Wong T-F. 1986. Mechanics of thermally induced cracking in three crustal rocks. Journal of Geophysical Research 91(B12):12743–54.

Ghassemi, A., Nygren A., and Cheng A.H.-D. 2008. Effect of Heat Extraction on Fracture Aperture: A Poro-Theromoelastic Analysis. Geothermics 37(5), 525-539.

Ghassemi, A., and Zhang, Q. 2006. Poro-thermoelastic response of a stationary crack using the displacement discontinuity method. ASCE Journal of Engineering Mechanics 132(1), 26-33.

Ghassemi, A., Tarasovs, S., and Cheng, A. H.-D. 2007. A three-dimensional study of the effects of thermo-mechanical loads on fracture slip in enhanced geothermal reservoir International Journal of Rock Mechanics & Mining Sciences & Geomechanics Abstracts 44, 1132–1148.

Goodman, R. E. 1976. Methods of Geological Engineering in Discontinuous Rocks, 1st Edition. St Paul, West Publishing Group, 472pp.

Julian, B.R., Foulger, Monastero F., C., Bjornstad, S. 2010. Imaging hydraulic fractures in a geothermal reservoir. Geophysical Research Letters 37, L07305.

Jung, R. 2013. EGS - Goodbye or back to the future, in Effective and Sustainable Hydraulic Fracturing, edited by A. P. Bunger, J. McLennan and R. Jeffrey, pp. 95-121, InTech, doi:10.5772/45724

Knapp, R.B., and Norton, D. 1981. Preliminary numerical analysis of processes related to magma crystallization and stress evolution in cooling pluton environments. American Journal of Science 281, 35–68.

Kohl T., Evans, K.F., Hopkirk, R.J., Ryback, L. 1995. Coupled hydraulic, thermal, and mechanical considerations for the simulation of hot dry rock reservoirs. Geothermics 24:345–59

Kurashige, M. 1989. A thermoelastic theory of fluid-filled porous materials. International Journal of Solids & Structures 25 (9), 1039–1052.

Li, X., Cui, L., Roegiers, J.-C. 1998. Thermoporoelastic modeling of wellbore stability in non-hydrostatic stress field. International Journal of Rock Mechanics & Mining Science 35, 4–5 Paper No. 063.

Majer, E.L. 2007. White Paper: Induced seismicity and enhanced geothermal systems. Center for Computational Seismology, Ernest Orlando Lawrence Berkelyey Laboratory, Berkelely, California, 32 pp.

McTigue, D.F. 1986. Thermoelastic response of fluid-saturated porous rock. Journal of Geophysical Research 91(B9), 9533–9542.

McTigue, D.F. 1986. Flow to a heated borehole in porous, thermoelastic rock: Analysis. Water Resources Research 26(8), 1763-1774.

Mossop, A. 2001. Seismicity, Subsidence and strain at the Geysers geothermal field. Ph.D. Dissertation, Stanford University. 51 pp.

Nowacki W. 1973. Thermoelasticity. New York: Pergamon Press.

Pearson, C. 1981. The relationship between micro-seismicity and high pore pressure during hydraulic stimulation experiments in low permeability rocks. Journal of Geophysical Research 86(B9), 7855- 7864.

Perkins, T.K. Gonzalez, J.A., 1985.The effect of thermoelastic stress on injection well fracturing. SPE Journal 2:78–88.

Pine, R.J., Batchelor, A.S. 1984. Downward migration of shearing in jointed rock during hydraulic injections. International Journal of Rock Mechanics & Mining Sciences & Geomechanics Abstracts 21(5), 249–63.

Rawal, A., and Ghassemi, A. 2014. A Reactive poro-thermoealstic analysis of cold water injection in enhanced geothermal reservoir. Geothermics, 50, 10-23

Safari, R., and Ghassemi, A. 2015. Three-dimensional thermo-poroelastic analysis of fracture network deformation and induced micro-seismicity in enhanced geothermal systems. Geothermics 58, 1-14

Segall, P., and Fitzgerald, S.D. 1998. A note on induced stress changes in hydrocarbon and geothermal reservoirs. Tectonophysics 289, 117–28

Stark, M.A. 1990. Imaging injected water in the Geysers reservoir using microearthquakes data. Geothermal Resources Council Transactions 14, 1697–704.

Tao, Q., Ghassemi, A., and Ehlig-Economides, C.E. 2011. A fully coupled method to model fracture permeability change in naturally fractured reservoirs. International Journal of Rock Mechanics & Mining Sciences & Geomechanics Abstracts, doi:10.1016/j.ijrmms.2010.11.012.

Tao, Q., and Ghassemi, A. 2010. Poro-thermoelastic borehole stress analysis for determination of the in-situ stress and rock strength, Geothermics 39 (30), 250-259.

Tao, Q., and Ghassemi, A. 2010. Simulation of fluid flow in naturally fractured poro-thermoelastic reservoirs. Proc. 35th Workshop on Geothermal Reservoir Engineering. Stanford University, Stanford, California.

Witherspoon, P.A., Wang, J.S.Y., Iwai, K., and Gale, J. E. 1980. Validity of cubic law for fluid flow in a deformable rock fracture. Water Resources Research 16, 1016-1024.